J. Fluid Mech. (2014), *vol.* 751, *pp.* 184–215.
doi:10.1017/jfm.2014.301

Drops of power-law fluids falling on a coated vertical fibre

Liyan Yu† and John Hinch

Department of Applied Mathematics and Theoretical Physics, University of Cambridge, Wilberforce Road, Cambridge CB3 0WA, UK

(Received 15 July 2013; revised 3 March 2014; accepted 22 May 2014; first published online 19 June 2014)

We study the solitary wave solutions in a thin film of a power-law fluid coating a vertical fibre. Different behaviours are observed for shear-thickening and shear-thinning fluids. For shear-thickening fluids, the solitary waves are larger and faster when the reduced Bond number is smaller. For shear-thinning fluids, two branches of solutions exist for a certain range of the Bond number, where the solitary waves are larger and faster on one and smaller and slower on the other as the Bond number decreases. We carry out an asymptotic analysis for the large and fast-travelling solitary waves to explain how their speeds and amplitudes change with the Bond number. The analysis is then extended to examine the stability of the two branches of solutions for the shear-thinning fluids.

Key words: non-Newtonian flows, solitary waves, thin films

1. Introduction

A cylinder of Newtonian fluid, a fluid with constant viscosity, undergoes a Rayleigh–Plateau instability in which surface tension breaks the cylinder into spherical drops to reduce the surface area. The wavelength of the instability is proportional to the radius of the cylinder. The time scale of the instability depends on whether the driving force of surface tension is resisted by inertia or viscosity. We shall be interested in viscously dominated dynamics.

For an axisymmetric film coating a circular cylindrical fibre, the presence of the fibre prevents the liquid from breaking into drops. Without gravity, the liquid film rearranges into bulges of length the circumference of the cylinder. The smaller bulges with the higher pressure then feed the growth of the large bulges (Hammond 1983).

When the fibre is vertical, gravity must be considered. The dynamics of the instabilities depend on the strength of the gravity, measured by a non-dimensional reduced Bond number, reduced to take account of the film being thin,

$$G = \frac{\rho g a^3}{\gamma h}, \tag{1.1}$$

where ρ is the liquid density, g the gravitational acceleration, a the fibre radius, γ the surface tension and h the film thickness. Quéré (1999) found in experiments with

† Email address for correspondence: liyanyuyu@gmail.com

Newtonian fluids that for small G, i.e. for films thicker than a critical value, the small bulges grew into large drops as they fell down the fibre, while for large G, i.e. thinner films, the bulges remain small and could be hardly observed. He found the critical value of G separating the two behaviours to be 0.71.

Kalliadasis & Chang (1994) studied the behaviour of Newtonian fluids using a lubrication approximation. They found numerically that for smaller G, small bulges grew to large pulses very quickly by leaving behind a thinner film than that in front of them. These pulses blew up in a finite time at t_* as t approaches, in a manner, suggested to be $O(t_* - t)^{-1/3}$, although later corrected to be $O(t_* - t)^{-2}$ by Chang & Demekhin (1999). For larger G, the initial disturbances developed into a train of steadily travelling solitary waves, each with the same amplitude and speed and with equal film thickness at the front and the back. Kalliadasis & Chang (1994) went on to present an asymptotic analysis of the large solitary waves under the lubrication theory and found the critical value of G separating the two cases to be 0.59. We have recently revisited their calculation (Yu & Hinch 2013). Ruyer-Quil & Kalliadasis (2012) studied a non-lubrication system of equations that takes some account of inertia and thicker films.

In this paper, we analyse the solitary wave solutions under the lubrication approximation when the coating fluid exhibits shear-thinning and shear-thickening behaviour. The initial growth of the small disturbances was found to be qualitatively similar to that of a Newtonian fluid by Boulogne, Pauchard & Giorgiutti-Dauphiné (2012) and Boulogne *et al.* (2013) through experiments and linear stability analysis. Their experiments were in the regime where G is relatively small. Hence, small bulges grew to large drops of size the order of the fibre radius in a short period time and the lubrication theory no longer applied. We address the problem of non-thin-film drops in another paper in preparation. Here, we shall focus entirely on G being larger than some critical value to be found.

The paper is structured as follows. The problem is formulated in § 2. The numerical results are presented in § 3 where distinct behaviours of the solitary wave solutions depending on the power-law index are observed. In particular, two branches of solutions exist for shear-thinning fluids. Section 4 introduces the first approximations of the large and fast solitary waves and §§ 5–7 present a full asymptotic analysis of them. The analysis is then extended in § 8 to examine the stability of the different branches of solutions for the shear-thinning fluids.

2. Governing equations

We consider a solid vertical fibre of radius a coated by an axisymmetric film of a power-law fluid of thickness $h(x, t)$, where x measures the axial distance downwards along the fibre (see figure 1). The film is assumed to be both thin with $h \ll a$ and vary along the fibre on the length scale of the fibre radius with $\partial h/\partial x \ll 1$. The capillary pressure in the film is γ/a at leading order, where γ is the surface tension. This constant pressure drives no flow. The flow is driven by small $O(\gamma h/a^2)$ corrections, which vary along the fibre, and which are typically negative corresponding to the film radius being larger than a. We shall ignore the leading-order constant and call instead this first correction 'the' capillary pressure. Thus in the thin-film approximation, our capillary pressure is

$$p = \gamma(-h/a^2 - h_{xx}). \tag{2.1}$$

The gradient of this capillary pressure along with gravity drives the flow down the fibre.

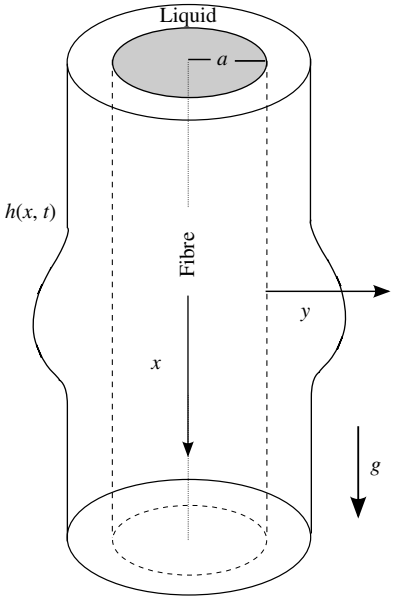

FIGURE 1. Schematic diagram.

The viscosity μ of the fluid is taken to have a power-law dependence on the shear rate, which is approximately $\partial u/\partial y$ in the thin-film approximation,

$$\mu = \beta \left| \frac{\partial u}{\partial y} \right|^{n-1}, \tag{2.2}$$

where β is a positive constant and y is the coordinate measuring across the thickness of the film. The power-law index n is less than one for shear-thinning fluid and greater than one for shear-thickening fluid. The case of Newtonian fluid is recovered when n is equal to 1. The modulus sign makes sure that the viscosity is always positive and the stress is in the same direction as the shear rate. The shear stress σ_{xy} thus can be written as

$$\sigma_{xy} = \beta \operatorname{sgn}\left(\frac{\partial u}{\partial y}\right) \left| \frac{\partial u}{\partial y} \right|^{n}. \tag{2.3}$$

For a thin film, the lubrication approximation gives the flux per unit circumference

$$q = \frac{n}{2n+1} \beta^{-1/n} h^{2+(1/n)} \operatorname{sgn}(\rho g - p_x) \, |\rho g - p_x|^{1/n} \tag{2.4}$$

where the sign of the pressure gradient $\rho g - p_x$ decides the direction of the flow. For the purpose of simplifying the presentation, we shall write the flux as

$$q = \frac{n}{2n+1} \beta^{-1/n} h^{2+(1/n)} (\rho g - p_x)^{1/n} \tag{2.5}$$

where a proper treatment of the modulus sign is assumed. Finally, mass conservation gives

$$h_t + q_x = 0. \tag{2.6}$$

We non-dimensionalise the axial position x by the fibre radius a, the film thickness $h(x, t)$ by an assumed initial uniform thickness h_∞, time t by the time scale of the viscous instability $((2n+1)/n)(\beta a^{n+3}/\gamma h_\infty^{n+2})^{1/n}$, and capillary pressure by $\gamma h_\infty/a^2$. With this non-dimensionalisation, the governing equation becomes

$$h_t + (h^{2+(1/n)}(G + (h + h_{xx})_x)^{1/n})_x = 0, \tag{2.7}$$

with the non-dimensional parameter the reduced Bond number $G = \rho g a^3/\gamma h_\infty$.

We are interested in solitary waves which propagate steadily at speed c without change of form, i.e. in solutions of the form $h(x - ct)$. Substituting this into the equation above, integrating once and applying the condition of the initial thickness far from the disturbance, we obtain the governing equation in the travelling wave frame

$$h^{2n+1}\,(G + (h + h_{xx})_x) = \left(c(h-1) + G^{1/n}\right)^n \quad \text{with } h \to 1 \text{ as } x \to \pm\infty. \tag{2.8}$$

We seek solutions of this equation. It is an eigenvalue problem, to find the eigenvalue of the speed for given Bond number $c(G)$ and the associated eigensolution for the shape $h(x)$.

3. Numerical results

Numerical solutions of the third-order nonlinear equation (2.8) have been obtained by shooting inwards from the far field at either side of the solitary wave to a common meeting point. The meeting point was chosen to be where $h_{xx} = 0$, $h_x < 0$ and h suitably greater than one, say $h > 1.2$. While the parameters had the wrong values, the solutions from the left of the meeting point had different values of h and h_x from those from the right.

In the far field with $h = 1 + \tilde{h}$ ($\tilde{h} \ll 1$), (2.8) can be linearised around the undisturbed thickness $h = 1$ to give

$$\tilde{h}''' + \tilde{h}' - (cnG^{1-(1/n)} - (2n+1)G)\tilde{h} = 0, \tag{3.1}$$

where primes denote differentiation with respect to x. The quantity $(cnG^{1-(1/n)} - (2n+1)G)$ is always positive for the solitary waves, since the implied $c = ((2n+1)/n)G^{1/n}$ is the speed of small interfacial disturbances. There are three solutions of exponential form for $\tilde{h}$. One grows exponentially as x increases and the other two grow exponentially in an oscillatory manner as x decreases. To find the eigensolution of $h(x)$ to the left of the meeting point, i.e. above the falling drop, we set the initial conditions of h, h_x and h_{xx} corresponding to the one solution of $\tilde{h}$ which grows exponentially with increasing x, starting at a very small amplitude. To find $h(x)$ to the right, i.e. below the falling drop, we start with a combination of the two linearised solutions which grow as x decreases, the ratio of the two different solutions being a free parameter. For a given G, this free parameter and the unknown speed c are adjusted iteratively until the solutions from the left and the right meet with h and h_x equal.

Figure 2 plots the solitary waves for $n = 0.8$ with $G = 0.9$ and 0.75. As in many cases, the amplitude increases as the Bond number G decreases, since the larger surface tension drives the instabilities to grow before the competing gravity carries the disturbances down. But there are exceptions to this which will be described in the next paragraph. The solitary waves are localised in the region $[0, 2\pi]$, with the higher amplitude wave decaying more rapidly into the far field.

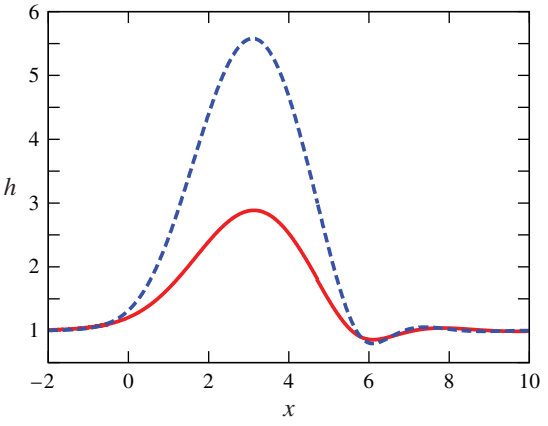

FIGURE 2. (Colour online) The shape of solitary waves $h(x)$. Both curves are for power-law index $n = 0.8$. The lower continuous curve is for $G = 0.9$ with $c = 9.3$ while the upper dashed curve is for $G = 0.75$ with $c = 18.8$.

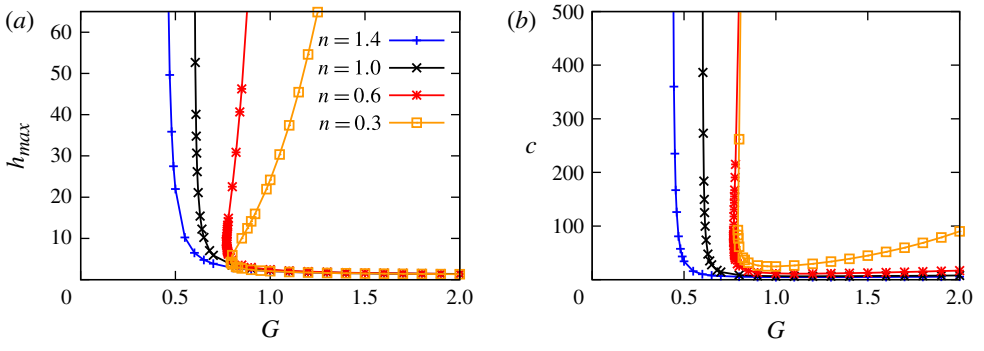

FIGURE 3. (Colour online) (*a*) The amplitude defined to be the maximum of $h(x)$ and (*b*) the speed c of the solitary waves as a function of G for $n = 1.4$, 1, 0.6 and 0.3.

Figure 3 plots as functions of the reduced Bond number G the amplitude h_{max}, defined to be the maximum value of $h(x)$, and the speed c. At large values of G, the amplitude h_{max} decreases to the uniform film thickness $h = 1$ while the speed c increases as $G^{1/n}$ since the large gravity suppresses the instabilities and speeds up the solitary waves. For the Newtonian fluid with $n = 1$ and the shear-thickening fluids with $1 < n < 1.5$, the amplitude grows monotonically without limit as G decreases to a critical value, below which there are no solitary wave solutions. In contrast, for shear-thinning fluids with $0.5 < n < 1$, the amplitude increases to a finite value as G decreases towards a minimum. There is then a range of G above this minimum where there are two branches of solitary waves. On the upper branch, the amplitude increases indefinitely as G increases towards the higher end of the range. The same is true for the more shear-thinning fluids with $0 < n < 0.5$, except that this higher end of the range is infinity and the two branches exist for all values of G above the minimum. The speed c also shows these three different behaviours for n in the different ranges. In this paper, we shall focus on the range $0 < n < 1.5$, which covers all the shear-thinning fluids and the common shear-thickening fluids.

4. First approximations

We are interested in the 'large' and 'fast' solitary waves. These waves can be divided into three regions: a 'main body' region in the middle where $h(x)$ is large and two transition regions at the front and back connecting the 'main body' to the far-field uniform film. Studying the leading-order approximations to these regions leads us to pose a matched asymptotic solution in terms of the small parameter $c^{-n/3}$. To fully solve the problem and find the relation between G and c, one needs to go to the second correction when $n \neq 1$ and the third correction when $n = 1$.

With h very large in the main body region of the solitary wave, the flux $h^{2n+1}(h + h_{xx})_x$ driven by the capillary pressure would dominate in (2.8) and so must be set equal to zero in the travelling wave frame. Hence the stabilising axial curvature balances with the destabilising azimuthal curvature and gives a steady drop of constant capillary pressure $-\kappa_0$. Hence,

$$h(x) \sim \kappa_0(1 - \cos x), \tag{4.1}$$

where we have chosen the solution to lie between $x = 0$ and $x = 2\pi$. We note in figure 2 that the region where h is large is the same for the two waves plotted and is approximately 2π long. The maximum height of the drop is $2\kappa_0$ and as the film thickness decreases to zero, it takes a parabolic shape

$$h(x) \sim \tfrac{1}{2}\kappa_0(x - x_0)^2, \tag{4.2}$$

where $x_0 = 0$ at the trailing left-hand side above the falling drop and $x_0 = 2\pi$ at the leading right-hand side below the falling drop.

As $h(x)$ drops from large values, viscous forces become important and the capillary pressure must change from its large value $-\kappa_0$ in the drop to the value -1 in the uniform film. The change occurs in a short transition region first investigated by Bretherton (1961) for bubbles advancing along a tube filled with a viscous liquid. When $h \sim O(1)$, the large $c^n(h - 1)^n$ term in (2.8) can be balanced if there are variations in x on the short scale $c^{-n/3}$. With the rescaling $x = x_0 + c^{-n/3}\xi$, the governing equation becomes at leading order the Bretherton equation modified for power-law fluid,

$$h_{\xi\xi\xi} = \frac{(h-1)^n}{h^{2n+1}}. \tag{4.3}$$

This needs to be solved numerically. As discussed for the numerical solutions in the previous section, one considers the equation of small disturbances to the uniform film to find a suitable initial condition for shooting. That equation turns out to be nonlinear because of the power law. It has some interesting features, which would however be a substantial digression at this stage, so they are presented in appendix B.

As h increases on entering the large drop, the term $h_{\xi\xi\xi}$ decreases and h takes a quadratic form

$$h \sim \tfrac{1}{2}P_{\pm}\xi^2 + Q_{\pm}\xi + R_{\pm} \tag{4.4}$$

with the plus subscript for $\xi \to +\infty$ in the trailing left-hand transition region and the minus subscript for $\xi \to -\infty$ in the leading right-hand transition region. The modified Bretherton equation has one free parameter in the left-hand transition region. Adjusting this free parameter, which is equivalent to an origin shift in ξ, one can make the linear term vanish to have $Q_+ = 0$. Then $P_+(n)$ and $R_+(n)$ are uniquely determined. Matching the above quadratic behaviour of $h(x)$ leaving the left-hand transition region with the quadratic behaviour found before at the left-hand end of the large drop, we

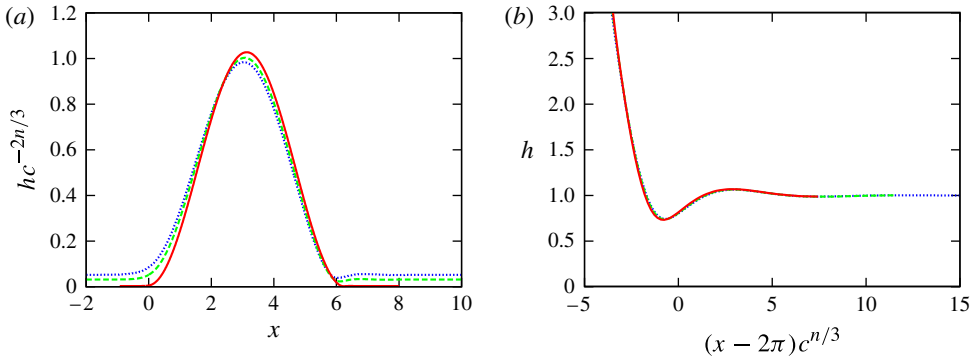

FIGURE 4. (Colour online) (*a*) The main drop. The shape $h(x)$ obtained numerically is scaled by $c^{-2n/3}$ for $G = 0.56$ (dotted), 0.54 (dashed) and 0.502 (solid). (*b*) The front transition region. The shape h obtained numerically is plotted as a function of the stretched variable $\xi = (x - 2\pi)c^{n/3}$ for $G = 0.56$ (dotted), 0.54 (dashed) and 0.502 (solid).

find a relation between the capillary pressure $-\kappa_0$ in the large drop and the speed c

$$\tfrac{1}{2}P_+c^{2n/3} = \tfrac{1}{2}\kappa_0. \tag{4.5}$$

The same matching at the right-hand end of the drop requires $P_- = P_+$. The modified Bretherton equation (4.3) has two free parameters in the right-hand transition region. One can again make the linear term vanish, $Q_- = 0$, and that leaves one degree of freedom so that R_- will vary as P_- varies. We hence force P_- to have the same value as P_+. Then R_- is determined. As P_+ and P_- are equal, we hereafter drop the subscripts.

The leading-order approximations show that the amplitude of the drop scales as $2Pc^{2n/3}$ and the width of the transition regions scales as $c^{-n/3}$. Figure 4(*a*) plots the computed shape $h(x)$ divided by $c^{2n/3}$ for three different values of G for $n = 1.2$. We observe that the rescaled shapes are very similar and that the maxima of 1.001, 1.024 and 1.027 are tending towards the predicted value of $2P = 1.023$ for $n = 1.2$ as G decreases towards the critical value. Figure 4(*b*) plots the shape $h(x)$ as a function of the stretched variable ξ for the right-hand transition region and the curves superpose well.

In the matching region between the transition region and the main drop, the shape is parabolic

$$h \sim \tfrac{1}{2}P\xi^2 + R_\pm = \tfrac{1}{2}Pc^{2/3}(x - x_0)^2 + R_\pm. \tag{4.6}$$

The values of P and $R_\pm$ are functions of the power-law index n. Figure 5 shows the values of P and $R_\pm$ for n varying in between 0 and 1.5. We see that P remains finite and decreases monotonically as n increases. The constant R_+ is always positive for $n > 0.5$ while R_- is negative.

The terms $R_\pm$ can be thought of as the effective film thickness of the uniform films at the back and the front as seen from within the large drop. For $0.5 < n < 1.5$, the larger R_+ corresponds to a lower capillary pressure at the left, or the top of the drop. The difference in pressure between the top and the bottom of the drop is the hydrostatic pressure gradient multiplied by the height difference 2π. Thus we conclude

$$G_0 = \frac{R_+ - R_-}{2\pi}. \tag{4.7}$$

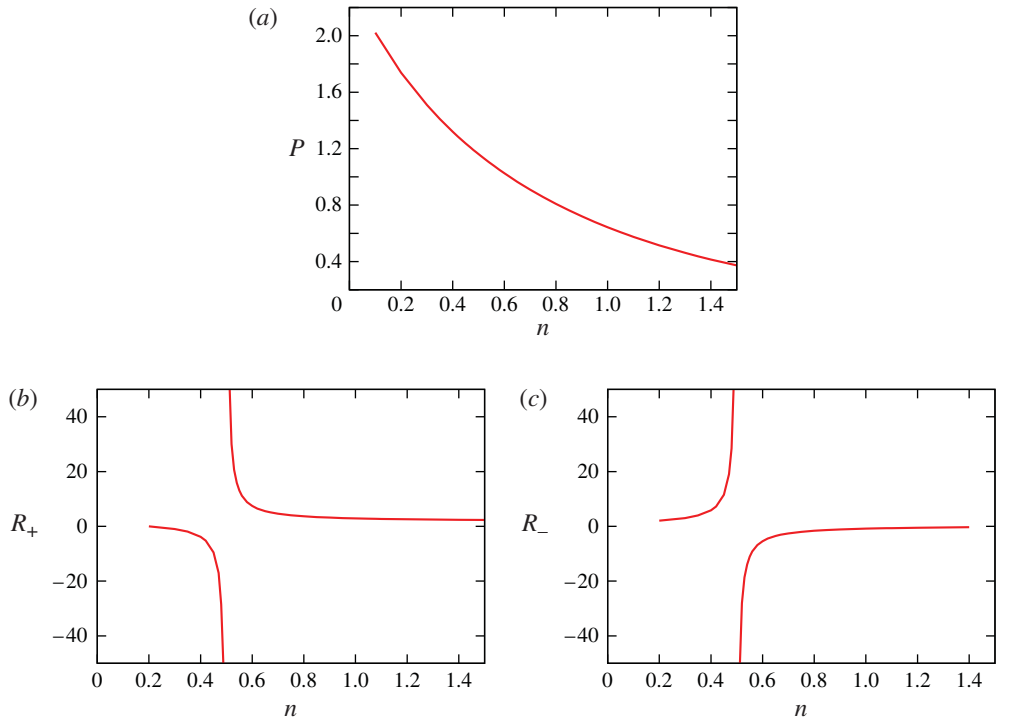

FIGURE 5. (Colour online) The values of the matching coefficients (*a*) P, (*b*) R_+ and (*c*) R_- as functions of the power-law index n.

For the Newtonian and shear-thickening fluid with $1 \leqslant n < 1.5$, this is the critical value of G_0 below which there are no solitary wave solutions. For the shear-thinning fluid with $0.5 < n < 1$, this is the critical value of G for the branch with the larger waves, above which there are no solitary wave solutions.

Curiously for the more shear-thinning fluids with $n < 0.5$, the capillary pressure $-R_+$ at the top of the drop is larger than that, $-R_-$, at the bottom. We will see in later sections that other physical effects from the main body region dominate over this hydrostatic pressure difference. We shall focus the analysis on n between 0.5 and 1.5 for now and will come back to the more shear-thinning fluids later, in § 7.8. Figure 6 plots the value of G_0 for $0 < n < 1.5$. It is positive and monotonically decreasing as n increases from 0.5 to 1.5. It then has negative values for n in $(0, 0.5)$.

The analysis so far yields a relation between the leading-order amplitude of the solitary wave and its speed. We have also found the critical value of G at which the amplitude and the speed blow up in the thin-film approximation for $0.5 < n < 1.5$. Once the thin-film assumption is relaxed, drops of the size of the fibre radius form and this critical value of G can be treated as an approximate boundary of G separating the smaller amplitude solitary waves and the larger drops. However, the relation between G and the speed c of the solitary waves remains to be determined and we shall find it by proceeding with the expansion of h in terms of a small parameter in both the transition regions and the main body region and then matching the expansions.

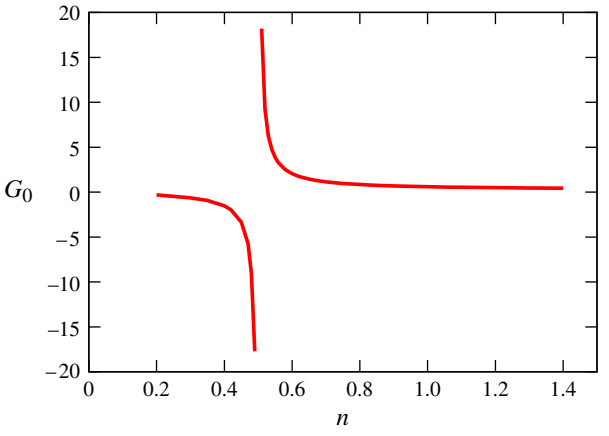

FIGURE 6. (Colour online) The critical value of G as a function of the power-law index n.

5. Transition regions

Although the control parameter for the problem is the reduced Bond number G and the unknown is the speed c of the solitary wave, it is more convenient to find G in terms of the small parameters of negative powers of c. Thus we pose

$$G \sim G_0 + c^{-n/3}0. \tag{5.1}$$

We have already found from the first approximations the critical value of G, G_0, for n between 0.5 and 1.5. We shall find shortly that there is no need for an $O(c^{-n/3})$ correction. Other correction terms are to be found in the calculations later.

With the rescaling $\xi = c^{n/3}(x - x_0)$ where $x_0 = 0$ for the left-hand trailing transition region and $x_0 = 2\pi$ for the right-hand leading transition region, (2.8) governing the solitary waves turns into

$$h_{\xi\xi\xi} = \frac{((h-1) + c^{-1}G^{1/n})^n}{h^{2n+1}} - c^{-2n/3}h_\xi - c^{-n}G. \tag{5.2}$$

This suggests an expansion

$$h \sim h_0 + 0c^{-n/3} + c^{-2n/3}h_2 + c^{-n}h_3 + c^{-1}h_4 + c^{-4n/3}h_5, \tag{5.3}$$

and we have checked that the solutions in the main body region do not force extra terms before h_5. Among the different orders, we shall see that h_0 and h_2 will determine the leading-order terms in the expansion of G while h_3, h_4 and h_5 give extra terms in the expansion of G but are too small to show a quantitative difference and hence are used mainly for ensuring the matching is correct. The terms h_3, h_4 and h_5 swap order depending on the value of n. This will not have a big impact on the matching and hence the result. We have arranged the terms assuming n is smaller than and close to 1.

5.1. *The leading order* h_0

The leading term h_0 satisfies the modified Bretherton equation

$$h_0''' = \frac{(h_0 - 1)^n}{h_0^{2n+1}} \tag{5.4}$$

n	P	R_+	R_-	a_2	c_{2+}	c_{2-}
1.4	0.4145	2.3957	−0.3133	−0.818	−17.92	14.73
1.3	0.4618	2.4741	−0.398 14	−0.883	−7.58	4.23
1.2	0.5450	2.5751	−0.5061	−0.965	−4.16	0.55
1.1	0.5750	2.7102	−0.6483	−1.072	−2.45	−1.60
1	0.6430	2.8996	−0.8453	−1.220	−1.33	−3.41
0.9	0.7203	3.1840	−1.1375	−1.439	−0.50	−5.60
0.8	0.8084	3.6577	−1.6192	−1.799	0.52	−9.16
0.7	0.9094	4.6039	−2.5736	−2.514	2.42	−18.43
0.6	1.0259	7.436	−5.413	−4.641	10.9	−62.6
0.4	1.3203	−3.84	5.86			
0.3	1.5093	−0.98	3.02			
0.2	1.7379	0.02	2.06			

TABLE 1. The values of the matching coefficients P, $R_\pm$, a_2 and and $c_{2\pm}$ for n between 0 and 1.5.

and has been discussed in detail in the previous section. As h becomes large on entering the main drop, it has asymptotic solution

$$h_0 \sim \tfrac{1}{2}P\xi^2 + R_\pm \pm k_1|\xi|^{1-2n} \tag{5.5}$$

where

$$k_1 = \frac{2^n}{P^{n+1}n(1-4n^2)}. \tag{5.6}$$

The plus sign is for the left-hand transition region as $\xi \to +\infty$ and the minus sign for the right-hand transition region as $\xi \to -\infty$. The first two terms were discussed earlier. The correction term was used when fitting to the numerical solution in order to extract accurate values of P and $R_\pm$. Fitting was performed over three ranges, (70, 120), (100, 150) and (120, 170). As n decreases from 1.5 to 0.5, the correction term becomes closer in order to the constant and for n less than 0.5, the correction term is larger than the constant. As a result, it was possible to produce more accurate estimates of $R_\pm$ when n is larger, with four significant decimal places for n around one and two for n around and less than 0.5. We list the values of P and $R_\pm$ in table 1.

5.2. *The first correction* h_2

At leading order in the transition region, the capillary pressure is dominated by the curvature along the axis, i.e. the term $-h_{xx}$. The curvature around the axis, the term $-h$, drives the first correction to the shape in the transition region, through the last term in the equation

$$h_2''' = \frac{(h_0-1)^{n-1}\,(-(n+1)h_0 + (2n+1))}{h_0^{2n+2}}h_2 - h_0'. \tag{5.7}$$

The asymptotic behaviour as the transition region merges into the main drop is

$$h_2 \sim -\frac{1}{4!}P\xi^4 + \frac{1}{2}a_{2\pm}\xi^2 \pm k_2|\xi|^{3-2n} + b_{2\pm}\xi + c_{2\pm}, \tag{5.8}$$

where

$$k_2 = \frac{2^{n-1}}{P^{n+1}(1-2n)(2-2n)(3-2n)}\left(\frac{n+1}{3} - \frac{2}{n(1+2n)}\right). \tag{5.9}$$

In anticipation of the matching, one can adjust the free parameters in the far fields to make the linear terms $b_{2\pm}\xi$ vanish and to make the two coefficients of the quadratic terms equal, $a_{2-} = a_{2+}$. The values of a_2 and $c_{2\pm}$ can then be determined by fitting the numerical solution to the asymptotic form over the three ranges (30, 50), (40, 60) and (50, 70). Two significant decimal places were obtained for n close to 1 and one decimal place for n close to 0.5. It is difficult to obtain more accurate numbers because h_2 becomes dominated by the large $-P\xi^4/4!$ term. The values of a_2 and $c_{2\pm}$ are included in table 1.

5.3. *Further terms*

We list here the equations and the asymptotic solutions for further terms in the transition region; they produce extra terms that ensure that the matching with the main body region is correct, but are not essential in giving the relation between G and c at the order we consider:

$$h_3''' = \frac{(h_0-1)^{n-1}(-(n+1)h_0+(2n+1))}{h_0^{2n+2}}h_3 - G_0, \tag{5.10}$$

$$h_4''' = \frac{(h_0-1)^{n-1}(-(n+1)h_0+(2n+1))}{h_0^{2n+2}}h_4 + \frac{n(h_0-1)^{n-1}G_0^{1/n}}{h_0^{2n+1}}, \tag{5.11}$$

$$h_5''' = \frac{(h_0-1)^{n-1}(-(n+1)h_0+(2n+1))}{h_0^{2n+2}}h_5 + \frac{h_0^2((h_0-1)^{n-2}h_2^2+2n+1)(2n+2)(h_0-1)^n}{2h_0^{2n+3}} - h_2'. \tag{5.12}$$

While the motion of the drop is eventually driven by gravity, G first appears in the $O(c^{-n})$ or $O(c^{-1})$ correction of the transition regions, depending on the value of n. The terms h_3 and h_4 merge when n is 1. The term h_5 is forced by the curvature along the fibre in h_2 in the same way as h_2 itself was forced by the curvature along the fibre in h_0. To the level of approximations required, they have solutions

$$h_3 \sim -\frac{1}{3!}G_0\xi^3 + \frac{1}{2}a_{3\pm}\xi^2 + b_{3\pm}\xi, \tag{5.13}$$

$$h_4 \sim \tfrac{1}{2}a_{4\pm}\xi^2, \tag{5.14}$$

$$h_5 \sim \frac{1}{6!}P\xi^6 - \frac{1}{4!}a_{2\pm}\xi^4 + k_3|\xi|^{5-2n} + \frac{1}{2}a_{5\pm}\xi^2, \tag{5.15}$$

where

$$k_3 = \frac{2^{n-1}}{P^{n+1}(3-2n)(4-2n)(5-2n)} \times \left(-\frac{8(n+1)}{6!} + \frac{1}{(1-2n)(2-2n)}\left(\frac{2}{n(1+2n)} - \frac{n+1}{3}\right)\right). \tag{5.16}$$

In anticipation of the matching and in a similar way as for h_0 and h_2, we can make the linear terms in these solutions vanish, with $b_{3\pm}$ equal to 0. We also make the coefficients of the quadratic terms equal in the two transition regions, with $a_{3+} = a_{3-}$, $a_{4+} = a_{4-}$ and $a_{5+} = a_{5-}$.

6. Main drop region

We rescale the film thickness in the main body region with the scaling law found in the first approximations, $h = c^{2n/3}H$, and rewrite the governing equation as

$$(H + H_{xx})_x = -c^{-2n/3}G + c^{-n(2n+1)/3}\frac{\left(1 - \dfrac{c^{-2n/3}}{H} + \dfrac{G^{1/n}(c^{-1-2n/3})}{H}\right)^n}{H^{n+1}}. \tag{6.1}$$

This leads us to expand H as

$$H \sim H_0 + 0c^{-n/3} + c^{-2n/3}H_2 + c^{-n(2n+1)/3}H_3 + c^{-n}H_4 + c^{-1}H_5 + c^{-4n/3}H_6. \tag{6.2}$$

The $O(c^{-2n/3})$ and $O(c^{-n(2n+1)/3})$ terms are forced by the respective relevant terms in the governing equation. They swap order, with $c^{-n(2n+1)/3}$ larger than $c^{-2n/3}$, for $n < 0.5$. We shall see from later sections that this explains the change in the relation between G and c for n greater and less than a half. The further $O(c^{-n})$, $O(c^{-1})$ and $O(c^{-4n/3})$ terms are forced by matching with the transition regions.

We again write G as

$$G \sim G_0 + c^{-n/3}0, \tag{6.3}$$

with the other correction terms to be found later.

6.1. *The leading order* H_0

In the first approximations, we have already found the leading-order term in the main drop

$$H_0 = P(1 - \cos x). \tag{6.4}$$

Because h is large, it must vanish at the two ends to become $O(1)$ there to match with the transition regions. The solution has a large constant capillary pressure $-c^{2n/3}P$.

6.2. *The first correction* H_2

The first correction has the hydrostatic pressure gradient. It is governed by

$$H_2' + H_2''' = -G_0 \tag{6.5}$$

and has the solution

$$H_2 = G_0(\sin x - x) + A_2 + C_2(1 - \cos x), \tag{6.6}$$

with constants A_2 and C_2 to be found by matching. In anticipation of the matching, we have already assumed a zero contact angle at the two ends with H_2' vanishing at $x = 0$ and 2π.

6.3. *The second correction* H_3

In the second correction, a pressure gradient drives a viscous return flow which cancels the unscaled flux ch. This term will eventually give the first approximation to how the speed c depends on G. The correction is governed by

$$H_0^{2n+1}(H_3 + H_3'')' = H_0^n. \tag{6.7}$$

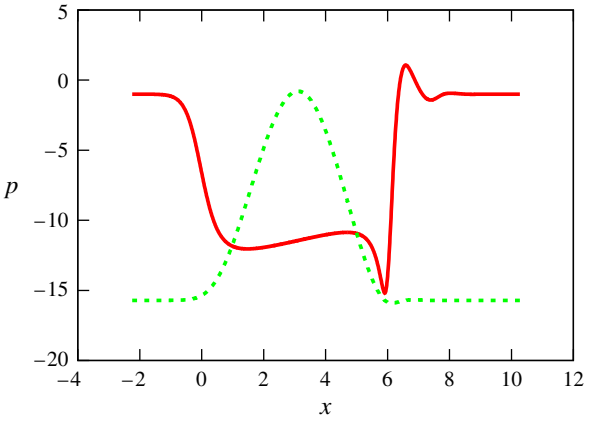

FIGURE 7. (Colour online) The pressure (continuous line) in the solitary wave for $n = 0.8$ and $G = 0.7$. The dotted line shows the position of the solitary wave.

The pressure gradient produced by H_3 is smaller at the centre of the drop because of the larger values of H_0 there. It then becomes larger in magnitude towards the transition region and eventually blows up like $(x - x_0)^{-2-2n}$ as H_0 vanishes at the two ends. To understand this, we notice that without any contribution from the pressure gradient, the flux of liquid in the thin film would vary as $-ch + G^{1/n}h^{2+1/n}$ in the frame moving with the wave. The pressure gradient keeps the flux equal to $-c + G^{1/n}$, its value in the uniform films, by acting against the backward flux. In the main drop where h is large, a very small pressure gradient suffices. However in the transition regions, a large pressure gradient is needed to drive the fluid back to the main drop through the very thin film at the two ends. As a result, H_3 blows up like $(x - x_0)^{1-2n}$ when n is greater than 0.5. However, this singular term in H_3 matches with the small correction term $\pm k_1|\xi|^{1-2n}$ in the expansion of h_0 in the transition regions. Hence, as we come out of the main drop region and enter the transition regions, other terms in the governing equation take over and regulate the blow-up behaviour in H_3 and hence in the pressure.

We plot in figure 7 the pressure variation in a solitary wave. In the uniform films after $(x < -1)$ and ahead $(x > 9)$ of the wave, the capillary pressure is -1. In the interior of the large drop $(1 < x < 5)$, the pressure is roughly constant, at a value of around our first prediction of $-\kappa_0 = -Pc^{2n/3} = -12.0$, using the computed value of $c = 157.19$. The small linear variation from the constant is due to the hydrostatic pressure in H_2. The pressure drops from -1 in the left-hand uniform film to the roughly constant value of -12 in a short transition region due to H_3, and then drops again to a minimum of -15 at the right-hand end of the drop. At the front of the pulse, there is a short region where the pressure gradient reverses sign. This makes the pressure rise to a positive maximum before approaching the uniform value -1 in an oscillatory fashion.

The equation governing H_3 can be solved numerically by shooting from the middle of the drop $x = \pi$ towards the two ends although care must be taken as x approaches the two singularities. We have avoided this problem by using some algebra to write H_3 as the sum of a singular part and a regular part,

n	D
1.4	−15.7871
1.3	−5.6458
1.2	−2.4388
1.1	−0.9145
1	0
0.9	0.6933
0.8	1.4071
0.7	2.4951
0.6	5.4079
0.4	−5.8161
0.3	−2.9818
0.2	−2.0428

TABLE 2. The values of D for n between 0 and 1.5.

$$\begin{aligned} H_3 \;=\; & \frac{n^2+n-1-n(n+1)\cos x}{P^{n+1}n(2n+1)(2n-1)}\frac{\sin x}{(1-\cos x)^n} \\ & + \frac{(n-1)(n+(n+1)\cos x)}{P^{n+1}(2n+1)(2n-1)}\int_{\pi}^{x}\frac{1}{(1-\cos t)^{n-1}}\mathrm{d}t \\ & + A_3 + B_3\sin x + C_3(1-\cos x). \end{aligned} \tag{6.8}$$

The first two terms form the particular integral. The first term is singular and is antisymmetric with respect to π. The integrand in the second term is not singular at the two ends if $n \leqslant 1$, so the integral can be calculated with ease. Expanding the solution of H_3 at the two ends gives

$$\begin{aligned} H_3 \;\sim\; & \pm k_1|x-x_0|^{1-2n} \pm D \pm k_2|x-x_0|^{3-2n} \pm k_3|x-x_0|^{5-2n} \\ & + A_3 + B_3(x-x_0) + \tfrac{1}{2}C_3(x-x_0)^2, \end{aligned} \tag{6.9}$$

where k_1, k_2 and k_3 were defined in § 5 for the transition regions. The integral term is odd with respect to π and D is the value of the integral when it is evaluated from π to 0. The plus sign in the solution is for $x_0 = 0$ and the minus sign is for $x_0 = 2\pi$. The coefficients k_1 and k_2 match the coefficients of the corrections of h_0 and h_2 in the transition regions. The difference in the constants $2D$ can be thought of as the pressure difference caused by the viscous flow inside the main drop. Numerically we find that $D < 0$ for the shear-thickening fluid with $1 < n < 1.5$ and $D > 0$ for the shear-thinning fluid with $0.5 < n < 1$. We found in a previous paper that $D = 0$ for the Newtonian case with $n = 1$. This suggest that this viscous pressure effect is related to the shear-thinning and shear-thickening properties of the fluids. It generates a negative pressure gradient in the main drop for $1 < n < 1.5$ and a positive one for $0.5 < n < 1$. Table 2 lists the values of D for different values of n. They blow up at $n = 0.5$. Again, we will leave the discussion of this special case to § 7.8.

We shall see from matching that no terms in the transition regions match the constants $\pm D$. As a result, a contribution from the gravitational term G is required to compensate for the difference in $\pm D$. By expanding G as

$$G \sim G_0 + c^{-n(2n-1)/3}G_1, \tag{6.10}$$

the correction H_3 then satisfies the new equation

$$H_0^{2n+1}(G_1 + H_3' + H_3''') = H_0^n, \tag{6.11}$$

with new solutions at the two ends

$$\begin{aligned} H_3 \sim\ & \pm k_1|x-x_0|^{1-2n} \pm D - G_1 x_0 \pm k_2|x-x_0|^{3-2n} \pm k_3|x-x_0|^{5-2n} \\ & + A_3 + B_3(x-x_0) + \tfrac{1}{2}C_3(x-x_0)^2. \end{aligned} \tag{6.12}$$

The value of G_1 is then determined as

$$G_1 = -\frac{D}{\pi}. \tag{6.13}$$

6.4. *The third correction H_4*

The third correction is not forced by the interior of the main drop but by matching, and hence is relatively straightforward. It is governed by

$$H_4' + H_4''' = 0 \tag{6.14}$$

and has the solution

$$H_4 = A_4 + B_4 \sin x + C_4(1 - \cos x) \tag{6.15}$$

with constants A_4, B_4 and C_4 to be found by matching.

6.5. *The fourth correction H_5*

Similarly to H_4, the fourth correction H_5 is also forced by matching. It satisfies

$$H_5' + H_5''' = 0, \tag{6.16}$$

with the solution

$$H_5 = A_5 + B_5 \sin x + C_5(1 - \cos x). \tag{6.17}$$

The constants are to be determined by matching.

6.6. *The fifth correction H_6*

The fifth correction is a copy of the first correction H_2 and is forced by a second correction term in the expansion of G. By expanding G as

$$G \sim G_0 + c^{-n(2n-1)/3}G_1 + c^{-2n/3}G_2, \tag{6.18}$$

the fifth correction H_6 is governed by

$$H_6' + H_6''' = -G_2, \tag{6.19}$$

and has the solution

$$H_6 = G_2(\sin x - x) + A_6 + B_6 \sin x + C_6(1 - \cos x). \tag{6.20}$$

The constants are to be found by matching.

The existence of the hydrostatic pressure $-G_2 x$ results in a difference in the film thickness at $O(c^{-2n/3})$ at the two ends of the drop. This difference is required to match the difference in the constants $c_{2\pm}$ in the solution of h_2 in the transition regions. We hence obtain the second approximation to how the speed c depends on G.

7. Matching

The transition regions had some free coefficients that we fixed in anticipation of the matching. The main drop region has a number of as yet undetermined constants, the As, Bs and Cs, as well as the important expansion of G. To match the expansion for the left-hand transition region as $\xi \to \infty$ to that for the main drop as $x \to 0$, we express the two asymptotic expansions in terms of $x = \xi c^{-n/3}$ and collect terms of the same order. The behaviour of the left-hand transition region is

$$\begin{array}{rccccccc}
 & h_0 & & h_2 & & h_3 & h_4 & h_5 & \\
c^{2n/3}\Big[& \dfrac{P}{2}x^2 & & -\dfrac{P}{4!}x^4 & & & & +\dfrac{P}{6!}x^6 & +\cdots \Big] \\
+c^{0}\Big[& R_+ & & +\dfrac{a_2}{2}x^2 & & -\dfrac{G_0}{3!}x^3 & & -\dfrac{a_2}{4!}x^4 & +\cdots \Big] \\
+c^{-(n(2n-1))/3}\Big[& k_1x^{1-2n} & & +k_2x^{3-2n} & & & & +k_3x^{5-2n} & +\cdots \Big] \\
+c^{-n/3}\Big[& & & & & +\dfrac{a_3}{2}x^2 & & & +\cdots \Big] \\
+c^{(2n/3)-1}\Big[& & & & & & \dfrac{a_4}{2}x^2 & & +\cdots \Big] \\
+c^{-2n/3}\Big[& & & c_{2+} & & & & +\dfrac{a_5}{2}x^2 & +\cdots \Big]
\end{array} \tag{7.1}$$

where k_1, k_2 and k_3 were defined in § 5. The columns give the contributions from the different terms from the solutions of the transition region, while the rows give terms of the same order in powers of c. The expansion above is for the left-hand transition region and is the same for the right-hand transition region, except that the $+$ subscripts are replaced by the $-$ subscripts for R_+ and c_{2+}, and x is replaced by $x - 2\pi$.

The behaviour of the main drop is

$$\begin{aligned}
&c^{2n/3}\left[\frac{P}{2}x^2 - \frac{P}{4!}x^4 + \frac{P}{6!}x^6 \ldots\right] \\
&+c^{0}\left[-G_0x_0 + A_2 + \frac{C_2}{2}x^2 - \frac{G_0}{3!}x^3 - \frac{C_2}{4!}x^4 + \cdots\right] \\
&+c^{-n(2n-1)/3}\left[k_1x^{1-2n} - G_1x_0 + D + A_3 + B_3x + k_2x^{3-2n} + \frac{C_3}{2}x^2 + k_3x^{5-2n} + \cdots\right] \\
&+c^{-n/3}\left[A_4 + B_4x + \frac{C_4}{2}x^2 + \cdots\right] \\
&+c^{(2n/3)-1}\left[A_5 + B_5x + \frac{C_5}{2}x^2 + \cdots\right] \\
&+c^{-2n/3}\left[-G_2x_0 + A_6 + B_6x + \frac{C_6}{2}x^2 + \cdots\right]
\end{aligned} \tag{7.2}$$

with the same k_1, k_2 and k_3. The rows come from the different H. The expansion above is for the left-hand end of the main drop with $x_0 = 0$. There is the same expansion around the right-hand end, with $+D$ replaced by $-D$, and all the x replaced by $(x - x_0)$ with $x_0 = 2\pi$.

7.1. *Matching at* $O(c^{2n/3})$

Matching at $O(c^{2n/3})$ is successful with the same powers of x present with the same coefficients. This is a consequence of the first approximations setting the calculation off in the correct direction.

7.2. *Matching at* $O(c^0)$

Matching at $O(c^0)$ gives from the constant terms $A_2 = R_+$ from the left-hand transition region and $-2\pi G_0 + A_2 = R_-$ from the right-hand transition region. This gives the critical value of the reduced Bond number $G_0 = (R_+ - R_-)/2\pi$. The x^2 and x^4 terms both give $a_2 = C_2$. The x^3 terms have the same coefficients.

7.3. *Matching at* $O(c^{-n(2n-1)/3})$

The x^{1-2n}, x^{3-2n} and x^{5-2n} terms have the same coefficients. There is no constant term from the transition regions. The left-hand end of the main drop gives $A_3 = -D$. The right-hand end of the main drop gives $-2\pi G_1 = D - A_3$. This gives the value of the first correction of the reduced Bond number $G_1 = -D/\pi$. There are no x and x^2 terms in the transition regions, which gives $B_3 = C_3 = 0$.

7.4. *Matching at* $O(c^{-n/3})$

Matching at $O(c^{-n/3})$ gives $A_4 = 0$ and $B_4 = 0$ from the constant and linear terms. The x^2 terms give $a_3 = C_4$.

7.5. *Matching at* $O(c^{2n/3-1})$

Matching at $O(c^{2n/3-1})$ gives $A_5 = 0$ and $B_5 = 0$ from the constant and linear terms. The x^2 terms give $a_4 = C_5$.

7.6. *Matching at* $O(c^{-2n/3})$

Matching at $O(c^{-2n/3})$ gives from the constant terms $A_6 = c_{2+}$ from the left-hand transition region and $-2\pi G_2 + A_6 = c_{2-}$ from the right. This gives the value of the second correction of the reduced Bond number $G_2 = (c_{2+} - c_{2-})/2\pi$. The x terms give $B_6 = 0$. The x^2 terms give $a_5 = C_6$.

7.7. *Matching results*

The orders corresponding to the different powers of c have been arranged with the assumption $0.5 < n < 1$ in the asymptotic expansions for the main drop and for the transition regions. The $O(c^{-n(2n-1)/3})$, $O(c^{-n/3})$ and $O(c^{2n/3-1})$ terms swap order for $1 < n < 1.5$, but this does not affect the result. All the terms have matched successfully. More importantly, we have obtained an expansion for the reduced Bond number G in terms of the speed c for $0.5 < n < 1.5$,

$$G \sim G_0 + c^{-n(2n-1)/3} G_1 + c^{-2n/3} G_2 \tag{7.3}$$

where

$$G_0 = \frac{R_+ - R_-}{2\pi}, \tag{7.4}$$

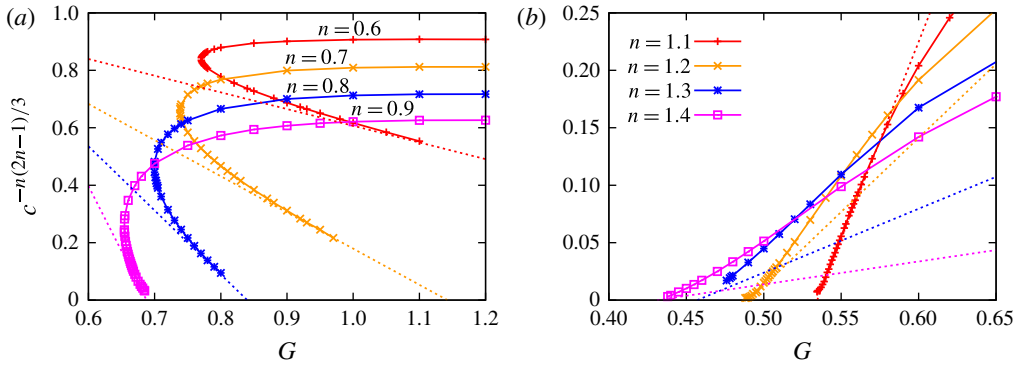

FIGURE 8. (Colour online) The speed c as a function of the reduced Bond number G for (*a*) $n < 1$ and (*b*) $n > 1$. The solid lines with points are the numerical solutions and the dotted straight lines are the first approximations using the first two terms in the expansion of G in (7.3).

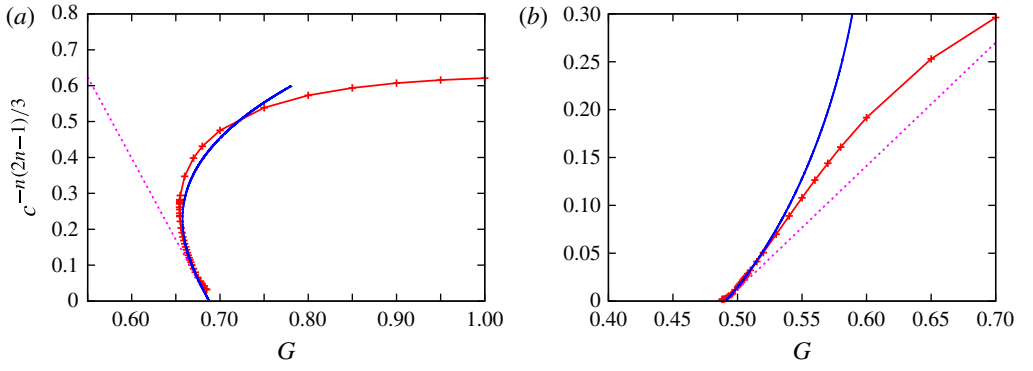

FIGURE 9. (Colour online) The speed c as a function of the reduced Bond number G for (*a*) $n = 0.9$ and (*b*) $n = 1.2$. The solid line with points is the numerical data, the dotted straight line is the first approximation and the plain solid line is the second approximation with all the three terms in the expansion of G.

$$G_1 = -\frac{D}{\pi}, \tag{7.5}$$

and

$$G_2 = \frac{c_{2+} - c_{2-}}{2\pi}. \tag{7.6}$$

Figures 8 and 9 plot $c^{-n(2n-1)/3}$ as a function of G, with the first two terms in the expansion giving the first approximation in figure 8 and all three terms giving the second approximation in figure 9. The first approximations lie tangent to the numerical solutions at the critical value G_0 and the second approximations improve on the first. The approximations work less well for n close to 1.5. This is because the order $c^{-n(2n-1)/3}$ of the G_1 term and the order $c^{-2n/3}$ of the G_2 term are equal at $n = 1.5$. Hence, the G_2 term is not a small correction for n close to 1.5.

The G_0 term was discussed in detail in § 4. We found that the terms $R_\pm$ leaving the transition regions could be thought of as the capillary pressure and the higher pressure

n	G_0	G_1	G_2
1.4	0.4312	5.0252	−5.20
1.3	0.4571	1.7971	−1.88
1.2	0.4904	0.7763	−0.75
1.1	0.5345	0.2911	−0.14
1	0.6430	0	0.33
0.9	0.6878	−0.2207	0.81
0.8	0.8399	−0.4479	1.54
0.7	1.1423	−0.7942	3.32
0.6	2.0447	−1.7214	11.7

TABLE 3. The values of G_0, G_1 and G_2 in the expansion of G for n between 0.5 and 1.5.

at the bottom is supplied by gravity. The difference in the capillary pressure $(R_+ - R_-)$ between the top and bottom of the large drop is balanced by the hydrostatic pressure difference $2\pi G_0$.

The H_3 correction in the main drop region provides a negative pressure gradient, i.e. larger pressure at the top of the pulse than at the bottom, to drive a viscous return flow inside the drop. This is to keep the flux everywhere the same as in the far field. The shear-thickening fluids are less viscous in the main drop because the shear rate is smaller in the main drop than in the transition regions. Thus less of the negative pressure gradient is required to drive the return flow for shear-thickening fluids. The extra negative pressure drop $2D$ is counteracted by the positive hydrostatic pressure drop $c^{-n(2n-1)/3}2\pi G_1$. For the shear-thinning fluids, the main drop region is more viscous. More negative pressure drop is needed to drive the return flow, which is supplied by a negative $c^{-n(2n-1)/3}2\pi G_1$. This explains the sign change of G_1 at $n=1$ in table 3.

A further pressure drop $c^{-2n/3}(c_{2+} - c_{2-})$ is produced by the h_2 correction in the transition regions. The h_2 term is forced by the curvature around the axis in h_0. This pressure drop is balanced by the $c^{-2n/3}2\pi G_2$ term.

Gravity first entered in the analysis in the correction H_2 and this yielded the value of the critical reduced Bond number G_0. Thus at this level of approximation the speed was unknown. It was then through the correction H_3 in the main drop region that c was first related to $G - G_0$. Thus for power-law fluids, the control of the speed depends on the viscous return flow in the main drop. For the Newtonian case $n=1$, the G_1 contribution is 0. The speed is then controlled by the G_2 term, from transition regions being corrected for the small effect of the curvature around the axis.

7.8. *The more shear-thinning fluid with* $0 < n < 0.5$

We have so far focused our analysis on $0.5 < n < 1.5$. We mentioned briefly in earlier sections that the terms in the asymptotic expansions swap order as n varies. A quick check on (7.3) shows that the $O(c^{-n(2n-1)/3})$ G_1 term becomes larger than the $O(1)$ G_0 term for $0 < n < 0.5$. We extend the previous analysis to $0 < n < 0.5$ in this section.

In the transition region, the leading order h_0 has the solution

$$h_0 \sim \tfrac{1}{2}P\xi^2 + R_\pm \pm k_1|\xi|^{1-2n} \tag{7.7}$$

where k_1 was given in § 5.1. The constants $R_\pm$ determined the leading-order term G_0 in the expansion of G for $0.5 < n < 1.5$. The $O(\xi^{1-2n})$ correction term is smaller than

n	G_1	G_0
0.4	1.8513	−1.54
0.3	0.9491	−0.64
0.2	0.6502	−0.32

TABLE 4. The values of G_1 and G_0 for some n less than 0.5.

the constant for $n > 0.5$ and becomes bigger than the constant when n is less than 0.5. We will see shortly that it is terms of this order in the main drop region that force a hydrostatic pressure drop, which dominates over the $O(1)$ pressure drop $2\pi G_0 = R_+ - R_-$.

The leading order in the main body region is still the same with $h \sim c^{2n/3}P(1 - \cos x)$, a steady drop with constant capillary pressure. The first correction is now the H_3 term that drives a viscous return flow in the main drop. This dominates over the other corrections to give

$$G \sim c^{n(1-2n)/3}G_1 \tag{7.8}$$

at leading order. The H_2 correction term then follows with the linear hydrostatic pressure variation across the drop matching with the constants $R_\pm$ in the solution of the modified Bretherton equation in the transition regions. We thus obtain

$$G \sim c^{n(1-2n)/3}G_1 + G_0. \tag{7.9}$$

The same symbols for G_1 and G_0 as in the last section are used to avoid confusion, although technically G_1 here is the leading-order term. It is not surprising that the $c^{-2n/3}G_2$ correction term in (7.3) is no longer the next correction for the expansion of G here. Instead, the next non-trivial solution in the main body region is forced by the viscous-pressure-related term H_3 and is likely to give a $c^{-4n^2/3}G_2$ correction to the expansion of G in (7.9). However, we will not pursue the expansion further since the result (7.9) already captures the main features.

We see in table 4 that G_1 is positive for n less than 0.5. Hence, the speed c grows indefinitely as G increases without limit. We plot G as a function of $c^{n(1-2n)/3}$ in figure 10 for $n = 0.4$. The theory appears to be a nice tangent to the curve of the numerical data as both c and G become bigger. It has been hard to obtain more data for larger values of G since the speed c increases very fast as G increases: the rightmost point on the graph corresponding to $G = 1.8$, which is a moderate value, has c of the order 10^{10}. This is mainly because the power $(n(1 - 2n)/3)$ in (7.9) is very small in magnitude for n less than 0.5 and hence the speed c changes by a large amount even as G varies little.

The hydrostatic pressure drop $c^{n(1-2n)/3}2\pi G_1$ balances the pressure difference $2D$ at the two ends produced by the viscous return flow in the main drop. The term $2\pi G_0$ provides the hydrostatic pressure to match with the $R_+ - R_-$ pressure difference in the transition regions. The transition regions have high shear rate compared to the main drop region and for $n > 0.5$ the pressure in the transition regions dominates. For $n < 0.5$, the fluids in the transition regions is significantly thinned and the flow in the main drop becomes more important, thus the change of order of G_0 and G_1. The values of $R_+ - R_-$ and $2D$ blow up and change signs at $n = 0.5$, but the different between the two, $(R_+ - R_-) - 2D$, remains finite. Perhaps one could think of the change of signs of G_0 and G_1 being related to their change of order.

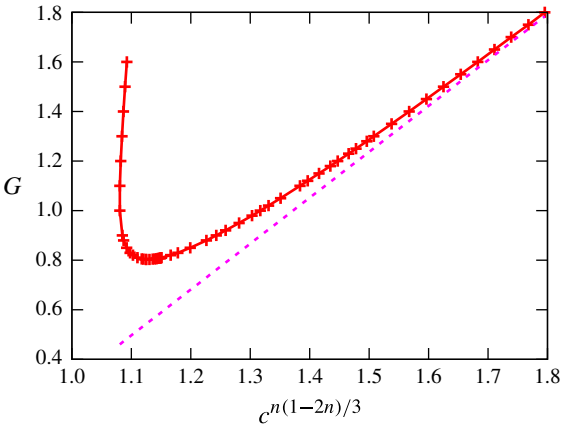

FIGURE 10. (Colour online) The reduced Bond number G as a function of $c^{n(1-2n)/3}$ for $n = 0.4$. The solid line with points is for the numerical data and the dotted line plots the asymptotic prediction using (7.9).

The case of $n = 0.5$ is yet to be discussed. We saw that G_0 and G_1 blow up at $n = 0.5$, and in the solution of h_0 in the transition regions the correction term appears to be of the same order as the constants. It turns out that logarithmic terms appear in the solutions of h for $n = 0.5$ and many details differ from the current solutions. We leave the calculation to appendix A for the interested reader.

8. Stability of the two branches for $0 < n < 1$

We have seen that two branches of solitary wave solutions exist for $n < 1$. In this section, we show that the upper branch of the solitary wave solutions, where the speed blows up as G increases, is unstable. This is done by extending the analysis carried out by Chang, Demekhin & Kalaidin (1995) for Newtonian fluids. They studied the ever-growing pulses at smaller values of G where solitary wave solutions do not exist. These pulses grow as they travel down the fibre by leaving behind a thinner film than the uniform film at the front. The growth of these pulses is a slow process and hence the asymptotic analysis for the solitary waves in the previous section can be easily extended to these quasi-steady pulses. We investigate how the film thicknesses at the front and at the back change for the solitary waves when the waves are perturbed slightly and whether the disturbances grow or shrink as a result.

The governing equation for the pulses with speed c in the travelling wave frame is

$$h_t + \left(h^3\left(G + (h + h_{xx})_x\right) - ch\right)_x = 0. \tag{8.1}$$

We assume a unit film thickness at the front and film thickness χ at the back,

$$h = 1 \quad \text{as } x \to \infty, \tag{8.2}$$

$$h = \chi \quad \text{as } x \to -\infty. \tag{8.3}$$

Integrating (8.1) from just after the pulse to just before the pulse, which is equivalent to a global mass balance, gives the scaling of the growth rate of the pulse when c is big, as $(\partial h/\partial t) = O(c(1-\chi))$. The thickness h in the main drop is $O(c^{2n/3})$ from the first approximations and this gives the time scale of the growth $t \sim O(c^{2n/3-1})$. We will see later that in both the transition regions and the main body region, the h_t term is negligible at our level of approximation.

8.1. *Transition regions*

For the left-hand transition region at the back of the pulse, (8.1) can be integrated from $x=-\infty$ where $h=\chi$ to give

$$h^{2+(1/n)}\,(G+(h+h_{xx})_x)^{1/n}=\chi^{2+(1/n)}G^{1/n}+c(h-\chi)-\frac{\partial}{\partial t}\int_{-\infty}^{x}h\,\mathrm{d}x. \tag{8.4}$$

In the transition region, the film thickness h is $O(1)$ and the width of the region is $O(c^{-n/3})$. We rescale the film thickness with $f=h/\chi$, the axial distance with $\xi=c^{n/3}x/\chi^{(n+2)/3}$ and obtain at leading order

$$f_{\xi\xi\xi}\sim\frac{(f-1)^n}{f^{2n+1}}-c^{-2n/3}\chi^{(2n+4)/3}f_{\xi}. \tag{8.5}$$

The evolution term $(\partial/\partial t)\int h\mathrm{d}x$ is of order c^{-n} in the above expansion and negligible. This leads us to follow § 5 and expand f as $f\sim f_0+c^{-2n/3}f_2$ with solutions of the form

$$f_0\;\sim\;\frac{1}{2}P_+\xi^2+R_+ +\frac{k_1}{P_+^{n+1}}\xi^{1-2n}, \tag{8.6}$$

$$f_2\;\sim\;-\frac{1}{4!}P_+\xi^4+\frac{1}{2}a_{2+}\xi^2+c_{2+}, \tag{8.7}$$

where k_1 was given in § 5.1 and the plus subscript is for $\xi\to+\infty$ for the left transition region. The film thickness h can then be expressed in terms of x as

$$\begin{aligned}h\;\sim\;&c^{2n/3}\left(\frac{P_+}{2\chi^{(1+2n)/3}}x^2-\frac{P_+}{4!\chi^{(1+2n)/3}}x^4\right)+c^0\left(R_+\chi+\frac{a_{2+}}{2\chi^{(1+2n)/3}}x^2\right)\\&+c^{-n(2n-1)/3}\left(\frac{k_1\chi^{(1+2n)(n+1)/3}}{P_+^{n+1}}x^{1-2n}\right)+c^{-2n/3}(c_{2+}\chi).\end{aligned} \tag{8.8}$$

A similar treatment is given to the right-hand transition region at the front of the pulse and it leads to

$$\begin{aligned}h\;\sim\;&c^{2n/3}\left(\frac{P_-}{2}(x-x_0)^2-\frac{P_-}{4!}(x-x_0)^4\right)+c^0\left(R_-+\frac{a_{2-}}{2}(x-x_0)^2\right)\\&+c^{-n(2n-1)/3}\left(-\frac{k_1}{P_-^{n+1}}|x-x_0|^{1-2n}\right)+c^{-2n/3}(c_{2-}),\end{aligned} \tag{8.9}$$

where $x_0=2\pi$ and the minus subscript is for $\xi\to-\infty$ for the front transition region.

The expansions of h are almost the same as that of the solitary waves in § 5, except that here we have accommodated for the change in the far-field film thickness at the back of the pulse.

8.2. *Main drop region*

In the main drop region, we integrate (8.1) from $x=-\infty$ where $h=\chi$ and from $x=+\infty$ where $h=1$ respectively to obtain

$$h^{2+(1/n)}(G+h_x+h_{xxx})^{1/n}-\chi^{2+(1/n)}G^{1/n}-c(h-\chi)+\frac{\partial}{\partial t}\int_{-\infty}^{x}h\,\mathrm{d}x\;=\;0, \tag{8.10}$$

$$h^{2+(1/n)}(G+h_x+h_{xxx})^{1/n}-G^{1/n}-c(h-1)-\frac{\partial}{\partial t}\int_x^\infty h\,\mathrm{d}x\;=\;0. \quad (8.11)$$

In the main drop, the film thickness is $O(c^{2n/3})$ and the width of the region is $O(1)$. The evolution term $(\partial/\partial t)\int h\,\mathrm{d}x$ is $O(c)$, small compared to the dominant $h^{2+(1/n)}G$, $h^{2+(1/n)}(h_x+h_{xxx})^{1/n}$, and ch terms in the equations. The terms with χ in them are also negligible. As a result, these two equations are identical at leading order, having the form

$$(h+h_{xx})_x=c^n\frac{h^n}{h^{2n+1}}-G. \quad (8.12)$$

The rest of the calculation in the main drop is the same as that in § 6. We rescale h with $c^{2n/3}H$ and expand H as

$$H\sim H_0+c^{-2n/3}H_2+c^{-n(2n+1)/3}H_3+c^{-4n/3}H_6, \quad (8.13)$$

where the $c^{-n}H_4$ and $c^{-1}H_5$ terms are not important and not written here for clarity of presentation. We also write G as

$$G\sim G_0+c^{-n(2n-1)/3}G_1+c^{-2n/3}G_2. \quad (8.14)$$

The terms H_0, H_2, H_3 and H_6 have the same solutions as in § 6 and the film thickness h can be expressed near the ends $x=x_0$ as

$$\begin{aligned}h\;\sim\;& c^{2n/3}\left(\frac{\kappa_0}{2}(x-x_0)^2-\frac{\kappa_0}{4!}(x-x_0)^4\right)+c^0\left(-G_0x_0+A_2+\frac{C_2}{2}(x-x_0)^2\right)\\&+c^{-n(2n-1)/3}\left(\pm\frac{k_1}{\kappa_0}|x-x_0|^{1-2n}-G_1x_0\pm\frac{D}{\kappa_0^{n+1}}+A_3\right)\\&+c^{-2n/3}(-G_2x_0+A_6),\end{aligned} \quad (8.15)$$

where $-\kappa_0$ is the pressure of the static drop solution of H_0 (and P was used instead of κ_0 in § 6.1 in anticipation of the matching). The constant D is defined slightly differently from those in § 6.3 with the $1/\kappa_0^{n+1}$ not included. We will see from matching that κ_0 changes with the back film thickness χ.

8.3. *Matching*

Matching at $O(c^{2n/3})$ gives $\kappa_0=P_-$ from the right-hand end of the drop and $\kappa_0=(P_+)/(\chi^{(1+2n)/3})$ from the left. This gives a relation between P_+ and P_-

$$\frac{P_+}{P_-}=\chi^{(1+2n)/3}. \quad (8.16)$$

The coefficients $P_\pm$ in the transition regions are no longer the same and instead depend on the film thickness χ at the back.

Matching at $O(c^0)$ gives from the constant terms $A_2=R_+\chi$ from the left-hand transition region and $-2\pi G_0+A_2=R_-$ from the right-hand transition region. This gives the critical value of the reduced Bond number $G_0=(R_+\chi-R_-)/2\pi$. We recall from § 4 that the values of $P_\pm$ and $R_\pm$ are determined by numerically solving the modified Bretherton equation. The values of P_+ and R_+ in the left-hand transition region are independent of the initial conditions and are uniquely determined. The

value of R_- varies as P_- varies in the right-hand transition region because of an extra degree of freedom. Once P_- is set to the value indicated by (8.16), the value of R_- will be uniquely determined. In other words, the value of R_- is a function of the film thickness χ at the back of the drop, and so is G_0 as a result. Matching the x^2 terms gives $a_{2+} = a_{2-}\chi^{(1+2n)/3}$.

Matching at $O(c^{-n(2n-1)/3})$ confirms (8.16) from the x^{1-2n} terms. There are no constant terms in the transition regions. The main drop region gives the first correction to the reduced Bond number $G_1 = -D/(\pi P_-^{n+1})$.

Matching at $O(c^{-2n/3})$ gives the second correction term to the reduced Bond number with $G_2 = (c_{2+} - c_{2-})/2\pi$.

Collecting together the results for G, we have

$$2\pi G = R_+\chi - R_- - c^{-n(2n-1)/3}2D/P_-^{n+1} + c^{-2n/3}(c_{2+}\chi - c_{2-}). \tag{8.17}$$

When $\chi = 1$, the previous result for the solitary waves is recovered. In the next subsection, we are going to test the stability of the pulse by examining how the film thickness χ at the back of the pulse changes when the amplitude h_{max} is slightly perturbed. To prepare for this, we rewrite the above equation in terms of h_{max} by using the first approximation $h_{max} \sim 2P_-c^{2n/3}$

$$R_- = -2\pi G + R_+\chi - h_{max}^{-(n-(1/2))}\chi^{n+(1/2)}P_+^{-(3/2)}2^{n+(1/2)}D. \tag{8.18}$$

We have re-expressed this equation as a relation between R_- and χ, the purpose of which will become clear later. The correction term of $O(c^{-2n/3})$ is left out because it is too small to affect the result. We have also used P_+ in the equation instead of P_- since P_+ is a constant that does not change with χ. The leading-order approximation for the amplitude h_{max} can be appropriately assumed as the correction terms are too small to change the stability result.

8.4. *Stability*

As discussed above, (8.16) gives one relation between R_- and χ for given values of G and h_{max}, since P_+ is uniquely determined from numerics and R_- only depends on P_-. Equation (8.18) gives another relation between R_- and χ. When R_- is plotted against χ using these two relations, the intersection of the two lines gives the value of χ at the specified G and h_{max}. Using the values of G and h_{max} of a numerically found solitary wave solution, one expects the intersection to be at $\chi = 1$.

We then perturb h_{max} slightly to see how the film thickness χ at the back changes. If χ becomes less than one, the pulse grows larger by leaving less fluid behind than it is collecting from the front. If χ is greater than one, the pulse shrinks by leaving more fluid behind. Mathematically, as h_{max} changes, the two lines corresponding to (8.16) and (8.18) intersect at another value of χ, which then enables us to tell the stability of the pulses.

Figure 11 illustrates the mechanism for $n = 0.8$ and $G = 0.78$. The two curves corresponding to the two relations cross at $\chi = 1$ when h_{max} equals the value of the corresponding solitary wave solution, representing equal film thickness at the front and the back as expected. When h_{max} is increased, the line for (8.18) moves upwards in the plot. This is because the $-D$ term in the equation is negative for $0.5 < n < 1$ and increasing the amplitude h_{max} increases the R_- for fixed χ. As a result, the new intersection is now at some χ less than one, which implies that the amplitude of the pulse keeps increasing. A similar argument applies when h_{max} is decreased. The

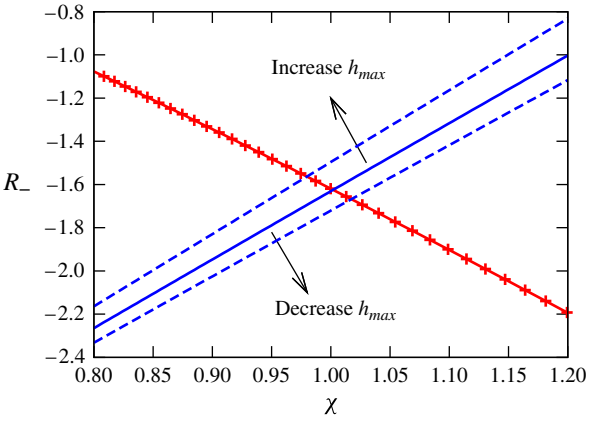

FIGURE 11. (Colour online) The mechanism of how χ changes when h_{max} varies. The solid line with crosses is the numerical data for how R_- changes with χ using (8.16). The other three lines plot the relation between R_- and χ using (8.18) at different values of h_{max} for $n=0.8$ and $G=0.78$. The middle solid line is when h_{max} equals its equilibrium value. The upper dashed line is for a bigger value of h_{max} and the lower dashed line is for a smaller value of h_{max}.

film thickness χ at the back increases and the pulse continues to shrink. We hence conclude that the upper branch of the solitary wave solutions for $0.5 < n < 1$ is unstable to small perturbations.

We found in §§ 6 and 7 that the pressure drop $2\pi G_1 = -2D$ is negative for $0.5 < n < 1$. It assists the viscous return flow in the main drop when the fluid in the main drop thickens due to smaller shear rate. When the amplitude h_{max} increases, the shear rate in the main drop decreases further and more of the negative pressure drop is needed. Hence the apparent film thickness at the front of the drop R_- increases to decrease the capillary pressure $-R_-$ there. The value of R_-, related to the film thickness at the front, is inversely correlated with χ the film thickness at the back. Hence χ decreases and the pulse keeps growing.

When n is less than 0.5, both (8.16) and (8.18) still apply. However, the power of the h_{max} term $-(n-(1/2))$ is now positive and D is negative for n in this range. As a result, R_- still increases as h_{max} increases. The back film thickness χ decreases and the pulse keeps growing. Similarly, the pulse reduces its volume further when h_{max} decreases. Hence, the upper branch of the solitary wave solutions for $n < 0.5$ is also unstable to perturbations.

8.5. *Turning point of the two branches for* $0.5 < n < 1$

The upper branch of the solitary wave solutions for $n < 1$ has been shown to be unstable and hence cannot be observed experimentally. It is then natural to look for the turning points of the two branches, i.e. the minimum value of G, G_m, at which stable solitary waves exist and can be observed (see figure 12). We plot the numerically found values of G_m for $0 < n < 1$ in figure 13. The values of G_m increases as n decreases from one. It then peaks at around 0.4 and decreases as n approaches zero. We have tried to estimate the value of G_m using the asymptotic expansion of G. It agrees well with the numerical data when n is close to one, but not so well when n is smaller.

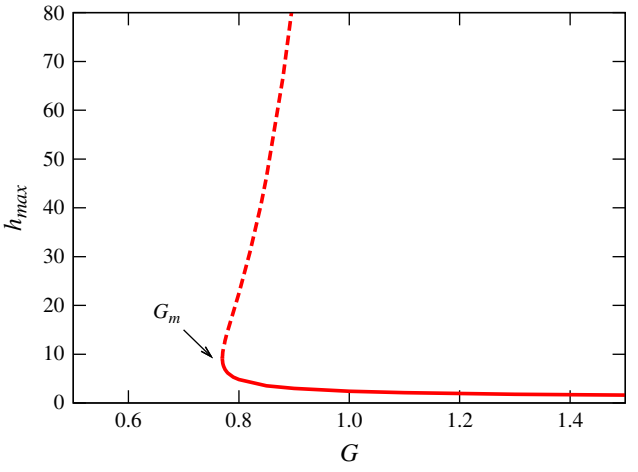

FIGURE 12. (Colour online) The turning point of the two branches at $G = G_m$ for $n = 0.6$.

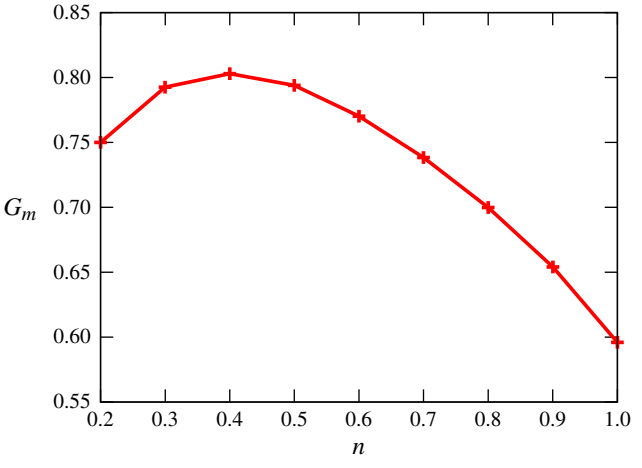

FIGURE 13. (Colour online) The numerical values of G at the turning point, G_m, as a function of the power-law index n.

9. Conclusion

We have looked at the 'large' and 'fast' solitary waves in a thin film of a power-law fluid coating a vertical fibre. The 'large' amplitude of the solitary waves does not violate the lubrication theory so long as $1 \ll h/h_\infty \ll a/h_\infty$. To fully solve the problem and find the relation between G and c, we needed to go to the second correction when $n \neq 1$ and the third correction when $n = 1$.

Fluids with the power-law index n varying between 0 and 1.5 have been studied. The asymptotic analysis of the large solitary waves gives the relation between the reduced Bond number G and the speed c of the waves. For $0.5 < n < 1.5$,

$$G \sim G_0 + c^{-n(2n-1)/3} G_1 + c^{-2n/3} G_2. \tag{9.1}$$

For the shear-thickening fluids with $1 < n < 1.5$, the first correction G_1 is positive. Hence the speed c blows up to infinity as G decreases towards the critical value

G_0. For the shear-thinning fluids with $0.5 < n < 1$, the correction G_1 is negative. Indeed in the numerical solutions, two branches of solutions have been observed for a certain range of G above a minimum value G_m. And on the upper branch, the speed c blows up as G increases towards the critical value G_0. For Newtonian fluid with $n = 1$, the value of G_1 is zero and hence G_2 gives the first correction of G. For the more shear-thinning fluids with $0 < n < 0.5$, we also obtained from the numerical constructions that there exist two branches of solutions of the solitary waves. The asymptotic analysis gives

$$G \sim c^{-n(2n-1)/3} G_1 + G_0. \tag{9.2}$$

The leading power of c is positive and G_1 is also positive. As a result, the speed c again increases with G indefinitely on the upper branch of the solitary wave solutions. The G_1 term comes from the viscous pressure drop in the low-shear-rate main drop while the G_0 term comes from high-shear-rate transition regions. For very shear-thinning fluids $0 < n < 0.5$, the viscosity is so small in the high-shear-rate transition regions that the viscous pressure drop there is smaller that from the main drop. For all the values of n studied, the amplitude h_{max} of the large solitary waves scales like $h_{max} \sim c^{2n/3}$.

For the two branches of the solitary wave solutions for $n < 1$, a similar asymptotic analysis is carried out on the large quasi-steady pulses. When the amplitude of the solitary waves is slightly increased, the film thickness left behind by the pulses has been found to decrease, and hence fuels the growth of the pulse, and vice versa. We conclude that the large solitary waves on the upper branch for the shear-thinning fluids are unstable.

Appendix A. Special case $n = 0.5$

The asymptotic analysis has some strange features when $n = 0.5$. The values of $R_\pm$ and D blow up and the leading terms in the expansions of G, G_0 and $c^{-n(2n-1)/3}G_1$, have the same order at $n = 0.5$. We show in this appendix that logarithmic terms appear in the expansions and G is of order $\log c$ at leading order for $n = 0.5$.

In the transition regions, the leading-order term h_0 has the form for $n \neq 0.5$

$$h_0 \sim \tfrac{1}{2} P\xi^2 + R_\pm \pm k_1 |\xi|^{1-2n}. \tag{A 1}$$

The correction term is obtained by inserting the first approximation $h_0 \sim \frac{1}{2}P\xi^2$ back into the governing modified Bretherton equation, giving $h_0''' \sim \pm(2^{n+1})/(P^{n+1})|\xi|^{-2-2n}$. This is then integrated three times to give the result. The correction term is smaller in order than the constant term for $n > 0.5$ and bigger than the constant for $n < 0.5$. When $n = 0.5$, it becomes a logarithm and h_0 takes the form

$$h_0 \sim \frac{P}{2}\xi^2 \pm \frac{2^{1/2}}{P^{3/2}} \log(|\xi|) + R_\pm, \tag{A 2}$$

where $R_\pm$ are constant terms which have to be found numerically.

Substituting $\xi = c^{n/3}(x - x_0) = c^{1/6}(x - x_0)$ for $n = 0.5$, we have at leading order

$$\begin{aligned} h \;\sim\; & c^{1/3}\left(\frac{P}{2}(x-x_0)^2\right) + \log c \left(\pm\frac{1}{3\sqrt{2}P^{3/2}}\right) \\ & + c^0 \left(\pm\frac{2^{1/2}}{P^{3/2}} \log(|x-x_0|) + R_\pm\right). \end{aligned} \tag{A 3}$$

We will see that the difference in the $O(\log c)$ terms in the two transitions regions forces an expansion of G at this order in the main body region.

In the main body region, the film thickness h is as usual rescaled using $h = c^{1/3}H$ for $n = 0.5$ and H satisfies

$$(H + H_{xx})_x = -c^{-1/3}\left(G - \frac{\left(1 - \dfrac{c^{-1/3}}{H} + \dfrac{G^2(c^{-4/3})}{H}\right)^{1/2}}{H^{3/2}}\right). \tag{A 4}$$

We expand H as

$$H \sim H_0 + c^{-1/3}\log c\, H_l + c^{-1/3}(H_2 + H_3) \tag{A 5}$$

where the $c^{-2n/3}H_2$ and $c^{-n(2n+1)/3}H_3$ terms from equation (6.2) have the same order of $c^{-1/3}$ for $n = 0.5$.

We have kept them separate to retain continuity from earlier discussions of the asymptotic expansions. The reduced Bond number G is expanded as

$$G \sim \log c\, G_l + G_0 \tag{A 6}$$

where the logarithmic term is to match with the transition regions.

The leading-order capillary static drop H_0 has the same form as before, $H_0 \sim P(1 - \cos x)$. The new correction term H_l is forced by G_l only and has solution

$$H_l = -G_l x + A_l + B_l \sin x + C_l(1 - \cos x). \tag{A 7}$$

At $O(c^{-1/3})$, H_2 has the hydrostatic pressure gradient with solution

$$H_2 = -G_0(x - \sin x). \tag{A 8}$$

The H_3 term driving a return flux in the main drop satisfies

$$H_3' + H_3''' = \frac{1}{P^{3/2}(1 - \cos x)^{3/2}}, \tag{A 9}$$

which was discussed in detail in § 6. This equation has an analytic solution of the form

$$H_3 = \frac{3}{2P^{3/2}}\frac{\sin x}{\sqrt{1 - \cos x}} + \frac{(3\cos x + 1)}{4P^{3/2}}\frac{2\sin(x/2)\log(2\tan x/4)}{\sqrt{1 - \cos x}}. \tag{A 10}$$

The solutions of H_2 and H_3 can be added to give the complete solution at $O(c^{-1/3})$. When expanded at the two ends, we have

$$H_2 + H_3 \sim -G_0 x_0 + D_\pm \pm \frac{2^{1/2}}{P^{3/2}}\log(|x - x_0|), \tag{A 11}$$

where $D_+ = (3 - 2\log 2)/\sqrt{2}P^{3/2}$ for $x_0 = 0$ and $D_- = (-3 + 6\log 2)/\sqrt{2}P^{3/2}$ for $x_0 = 2\pi$.

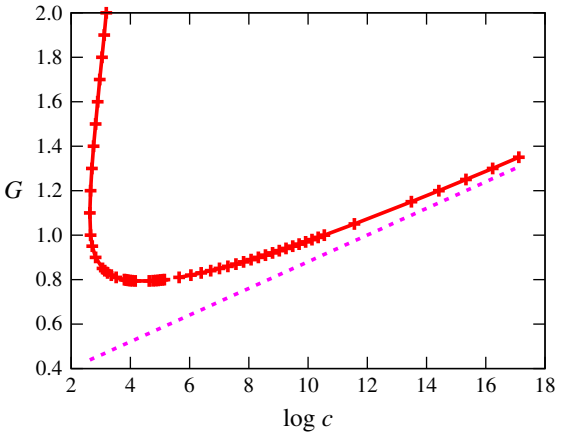

FIGURE 14. (Colour online) The reduced Bond number G as a function of $\log c$ for $n = 0.5$. The solid line with points is for the numerical data and the dotted line plots the asymptotic prediction using (A 15).

The film thickness in the main drop region thus has the expansion

$$h \sim c^{1/3}\left(\frac{P}{2}(x - x_0^2)\right) + \log c\,(-G_l x_0) + c^0\left(\pm\frac{2^{1/2}}{P^{3/2}}\log(|x - x_0|) - G_0 x_0 + D_\pm\right). \tag{A 12}$$

Matching at $O(\log c)$ gives the leading term in the expansion of G

$$G_l = \frac{1}{3\sqrt{2}P^{3/2}\pi}. \tag{A 13}$$

We find $P = 1.1613$ which gives $G_l = 0.060$.

Matching at $O(c^0)$, the log-terms are the same. The constant terms give

$$G_0 = \frac{R_+ - R_- - (D_+ - D_-)}{2\pi}. \tag{A 14}$$

It was mentioned in the first approximations in § 4 that the values of $R_\pm$ blow up as n becomes close to 0.5 (see figure 5). This could be the result of the $O(\xi^{1-2n})$ correction term becoming closer to the constant terms $R_\pm$ and actually becoming a logarithm at $n = 0.5$ in the solution of h_0. Here we have separated the logarithmic terms from the constants in the solution of h_0 and the values of $R_\pm$ are found to be finite, with $R_+ = 2.117$ and $R_- = 0.097$. This gives $G_0 = 0.28$.

In summary, when $n = 0.5$, the reduced Bond number G can be expressed as an expansion of c as

$$G = \log c\, G_l + G_0 \tag{A 15}$$

where $G_l = 0.060$ and $G_0 = 0.28$. We plot G as a function of $\log c$ in figure 14. The dotted theoretical prediction agrees well with the numerical data for larger values of G and c.

We have established that there are two branches of solitary wave solutions for n less than one. On the upper branch, the amplitudes and the speeds blow up at a finite value of G for $0.5 < n < 1$ whereas they roughly follow some power law of G as G increases indefinitely for $n < 0.5$. The case $n = 0.5$ is a boundary between these two and we have shown that G increases as the log of c at large values. Hence, as the speed c increases, the reduced Bond number G increases indefinitely again, but at a slower rate than it does for $n < 0.5$.

Appendix B. Discussion of the modified Bretherton equation

In this appendix, we discuss the equation of small disturbances to the modified Bretherton equation. It has been used to find the appropriate initial conditions for shooting the modified Bretherton equation but in itself possesses some interesting features. We write $h = 1 + \tilde{h}$ ($\tilde{h} \ll 1$) and neglect terms of order $\tilde{h}^2$ and higher. The modified Bretherton equation turns into

$$\tilde{h}''' = \tilde{h}^n. \tag{B 1}$$

When $n = 1$, the equation is linear and has three solutions of exponential form: e^{ξ}, $\mathrm{e}^{-\xi/2}\cos(\sqrt{3}/2)\xi$ and $\mathrm{e}^{-\xi/2}\sin(\sqrt{3}/2)\xi$. The first solution grows as ξ increases and is used for shooting towards $\xi \to +\infty$ in the left-hand transition region; the other two oscillate and grow as ξ decreases and are used for shooting towards $\xi \to -\infty$ in the right-hand transition region. However, the equation is nonlinear for $n \neq 1$ and there are no exponential solutions to (B 1).

For the left-hand transition region, one can seek a power-law solution. One finds

$$\tilde{h} = A(\xi - \xi_0)^{3/(1-n)}, \quad \text{in } \xi > \xi_0 \text{ for } n < 1, \tag{B 2}$$

$$\tilde{h} = A(\xi_0 - \xi)^{3/(1-n)}, \quad \text{in } \xi < \xi_0 \text{ for } n > 1, \tag{B 3}$$

where $A^{n-1} = 3(2+n)(1+2n)/|1-n|^3$. Both solutions grow as ξ increases and the second one blows up as ξ approaches ξ_0. In contrast to the Newtonian case where $\tilde{h}$ decreases exponentially to 0 as ξ decreases, the small disturbance $\tilde{h}$ reaches zero at a finite distance at $\xi = \xi_0$ for shear-thinning fluids and decays algebraically for shear-thickening fluids as $\xi \to -\infty$. As the disturbance decays with ξ decreasing, the shear rate decreases and so for shear-thinning fluids, the viscosity increases; it increases sufficiently for the disturbance to be damped in a finite distance. On the other hand for shear-thickening fluids, the viscosity decreases as the disturbance decays and so the disturbance decays slower than exponentially.

We have not found analytic solutions of (B 1) for the right-hand transition region at the front of the solitary wave. Numerically, the equation can be solved by shooting towards negative ξ from arbitrary initial conditions. The solutions oscillate around $\tilde{h} = 0$ and the amplitudes of these oscillations grow as ξ becomes more negative (figure 15*a*). The shapes of the oscillations, lying between each crossing of $\tilde{h} = 0$, are self-similar. For each of them, we rescale $\tilde{h}$ using their respective amplitudes and the axial distance using their lengths and figure 15(*b*) shows that they overlap perfectly. Varying the initial conditions will change the actual values of the amplitude and the length, but does not affect the characteristic shape. We write $\mathscr{H}$ and $\mathscr{L}$ for the characteristic height and length of these oscillations. A simple scaling argument from (B 1) gives $\mathscr{H}^{1-n} \sim \mathscr{L}^3$. Indeed for these oscillations, when the amplitude raised to

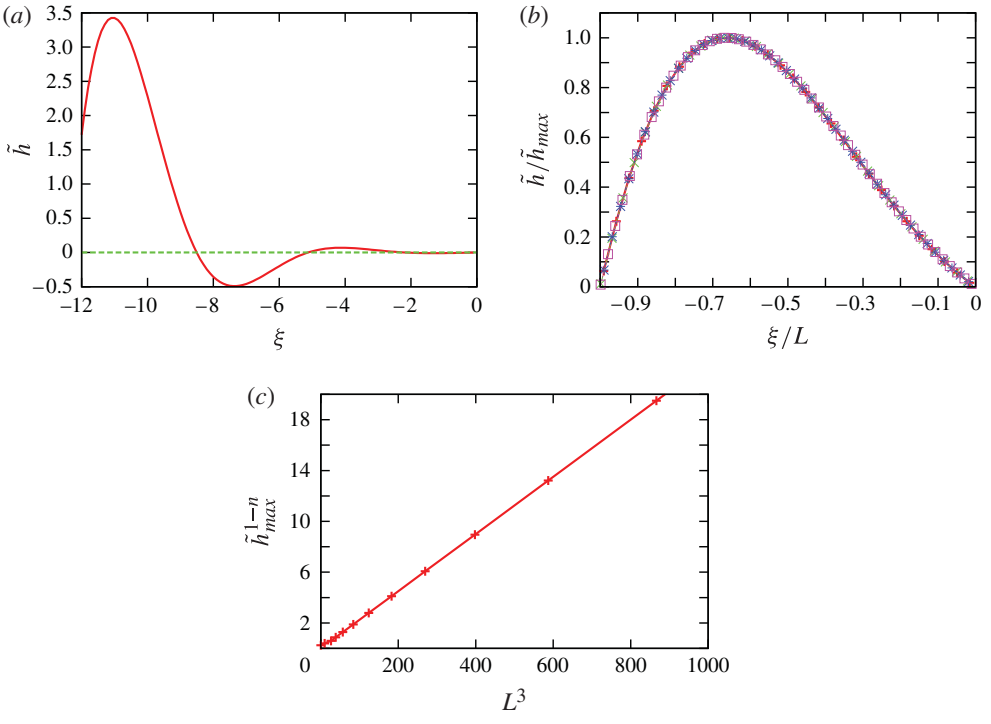

FIGURE 15. (Colour online) (*a*) Solution of (B 1) in the front transition region for $n = 0.8$. (*b*) The oscillations scaled with their amplitudes and lengths. (*c*) The amplitudes raised to the power $1 - n$ against the cube of the length of these oscillations.

the power $1 - n$ is plotted against the cube of the length in figure 15(*c*), a straight line goes through the data points. This scaling along with the continuity of $\tilde{h}'$ at the end and beginning of adjacent half-cycles implies that the half-wavelengths decrease by a factor $(-s_0/s_{-1})^{(2+n)/(3-n)}$ where s_0 and s_{-1} are the slopes in figure 15(*b*) at $\xi/L = 0$ and -1. Summing this geometric progression of the wavelengths, we conclude that the oscillation decreases to zero in a finite distance (while governed by (B 1)).

Equation (B 1) is an approximation to the modified Bretherton equation for when $\tilde{h}$ is small. We numerically solved the modified Bretherton equation to determine the coefficients P_-, Q_- and R_- of its asymptotic solution as $\xi \to -\infty$ in the front transition region. Its solution behaves like the solution of (B 1) initially, growing in an oscillatory manner, until the disturbance $\tilde{h}$ becomes large enough as it comes out of some oscillation. The value of the curvature term P_- as $\xi \to -\infty$ thus depends on the angle at which $\tilde{h}$ comes out from the final oscillation, which in turn is determined by the initial condition. We hence vary the initial conditions of h' and h'' iteratively to set P_- to P_+, the value of the curvature at the back transition region.

REFERENCES

BOULOGNE, F., FARDIN, M. A., LEROUGE, S., PAUCHARD, L. & GIORGIUTTI-DAUPHINÉ, F. 2013 Suppression of Rayleigh–Plateau instability on a vertical fibre coated with wormlike micelle solutions. *Soft Matt.* **9**, 7787–7796.

BOULOGNE, F., PAUCHARD, L. & GIORGIUTTI-DAUPHINÉ, F. 2012 Instability and morphology of polymer solutions coating a fibre. *J. Fluid Mech.* **704**, 232–250.

BRETHERTON, F. P. 1961 The motion of long bubbles in tubes. *J. Fluid Mech.* **10**, 168–188.

CHANG, H.-C. & DEMEKHIN, E. A. 1999 Mechanism for drop formation on a coated vertical fibre. *J. Fluid Mech.* **380**, 233–255.

CHANG, H.-C., DEMEKHIN, E. & KALAIDIN, E. 1995 Interaction dynamics of solitary waves on a falling film. *J. Fluid Mech.* **294**, 123–154.

HAMMOND, P. S. 1983 Nonlinear adjustment of a thin annular film of viscous fluid surrounding a thread of another within a circular cylindrical pipe. *J. Fluid Mech.* **137**, 363–384.

KALLIADASIS, S. & CHANG, H.-C. 1994 Drop formation during coating of vertical fibres. *J. Fluid Mech.* **261**, 135–168.

QUÉRÉ, D. 1999 Fluid coating on a fibre. *Annu. Rev. Fluid Mech.* **31**, 347–384.

RUYER-QUIL, C. & KALLIADASIS, S. 2012 Wavy regimes of flow down a fibre. *Phys. Rev.* E **85**, 046302.

YU, L. & HINCH, E. J. 2013 The velocity of 'large' viscous drops falling on a coated vertical fibre. *J. Fluid Mech.* **737**, 232–248.